Lasers in Manufacturing Conference 2021

Laser cleaning as a productive surface post-treatment method for L-PBF parts

Markus Hofele[a,b,*], Johannes Neuer[a], Malena Lindenberger-Ullrich[a], Jochen Schanz[a,b], David K. Harrison[b], Anjali K. M. De Silva[b], Harald Riegel[a]

[a]*Aalen University, Beethovenstraße 1, 73430 Aalen, Germany*
[b]*Glasgow Caledonian University, Cowcaddens Road, G4 0BA Glasgow, Scotland (UK)*

Abstract

The additive manufacturing technique Laser Powder Bed Fusion (L-PBF) offers the opportunity to directly build solid metal parts with less geometric restrictions, low porosity and good mechanical properties. However, the surface of the parts exhibits a rough surface with massive adherent powder combined with an oxide layer on it. Laser cleaning provides the possibility of a contact-free and full-automatable surface treatment with high area rates.
This work deals with the investigation on laser cleaning of L-PBF surfaces made of Aluminium AlSi10Mg. The laser cleaning is investigated with a nanosecond pulsed fibre laser by variation of the pulse energy and single pulse fluency. The ablation efficiency is analysed by means of SEM, WLI and microscopic images. Dust and oxide layers can be effectively removed. Adherent powder particles can be partly removed. Fluencies more than 13.2 mJ/mm² are causing surface remelting and beyond 30.8 mJ/mm² surface structuring occurs.

Keywords: Additive Manufacturing; Laser Powder Bed Fusion (L-PBF); Post-Processing; Laser Cleaning; Surface-Treatment

1. Introduction

The additive manufacturing technique Laser Powder Bed Fusion (L-PBF) offers the possibility of manufacturing complex 3D metallic parts with applications in various fields i.e. medical, automotive industry or aerospace (Denti et al., 2019, Guo et al., 2017, Nasab et al., 2018). Beside great chances offered through this technology, there are some disadvantages that hinder a more cost efficient application. L-PBF parts suffer

* Corresponding author.
E-mail address: markus.hofele@hs-aalen.de .

from a surface with loose and partially molten powder particles, spatters and ballings accompanied by oxide layers (Nasab et al., 2018, Townsend et al., 2016). These characteristics do often not measure up with industrial requirements (Metelkova et al., 2021). Partially molten particles can even be dangerous, for example in medical use where they entail a risk of peeling off from implants and being a threat to the patient (Guo et al., 2017).

Oxide layers on metals often need to be removed in a pre-treatment step as surface preparation before other laser material processing methods such as laser welding to improve quality (Zhu et al., 2019).

The above mentioned drawbacks of the L-PBF process lead to the necessity of post processing. Unwanted loose powder can for instance be removed by ultrasonic cleaning. Other ways to eliminate lose particles are acoustic cleaning, cleaning with mechanical vibrations (Seiffert et al., 2015), air pressure (Kolb et al., 2019) or laser induced shock waves (Metelkova et al., 2021).

For the removal of partially molten particles and oxide layers, other techniques are applied. All of these cleaning methods show disadvantages compared to the laser cleaning process. Among others, chemical cleaning methods are used (Guo et al., 2017, Kelly et al., 2019). The obvious disadvantage is the environmental damage caused by using chemicals, furthermore the costs created by the disposal of the chemicals cannot be neglected. Additionally, chemical methods such as surface etching can lead to a reduction of the thickness of the parts (Pehlivan et al., 2020). Another way to clean L-PBF metal parts is sandblasting (Guo et al., 2017). One of its drawbacks is that sandblasting does not offer the possibility of precise partial cleaning. In addition, for sandblasting there is a supplementary step needed to collect and dispose the residual abrasive material, which makes the process more time consuming. Similar to the sandblasting process snow blasting uses compressed air combined with CO_2 ice particles for the cleaning process, a rather loud method where gaseous CO_2 is released (Stark, 2021). Additively manufactured parts can also be cleaned with electroplasma based methods (Guo et al., 2017). The disadvantages are described by Guo et al. as “uneven removal” and “damage to the framework”.

The laser cleaning process combines a numerous amount of advantages. It is fast, precise and reduces the risk of generating mechanical forces as it is a contact free method, the process is versatile, controllable, dry, selective and environmentally friendly due to the absence of chemicals or other additives (Marimuthu et al., 2018, Wang et al., 2019, Razab et al., 2018). Further the process causes no noticeable loss of base material.

This paper deals with investigations on laser cleaning of L-PBF AlSi10Mg parts with a nanosecond pulsed fibre laser. Therefor parameter studies by varying the beam diameter, pulse repetition rate and pulse energy are performed. Threshold single pulse fluencies for powder particle removal, base material melting and surface structuring are determined. The cleaning and ablation efficiency is analysed by means of SEM, WLI and microscopic images.

2. Experimental set-up

The investigations on laser cleaning are done by means of vertically printed rectangular plates with the dimension of 80 mm length, 50 mm width and a material thickness of 3 mm. The Laser Powder Bed Fusion (L-PBF) printing process was executed on a TruPrint 1000 Multilaser (TRUMPF, Ditzingen, Germany) with two 200 W infrared fibre lasers. The machine has a cylindrical fabrication volume with a diameter of 100 mm and 100 mm in height. The experimental investigations are executed on Aluminium alloy AlSi10Mg. The used Aluminium powder by the company Heraeus exhibits a particle size distribution of D10 = 21.3 µm to D90 = 56.9 µm. The average powder grain diameter is 35.7 µm. The samples were built with recommended fabrication parameters, with a slicing thickness of 20 µm. The layers are molten on the outer contour by 175 W

laser power and a beam velocity of 2000 mm/s. The core of the parts is manufactured with 175 W, resp. 1400 mm/s and a hatch distance of 120 µm. During the fabrication process the chamber is flooded with Argon with a residual oxygen content of <0.3%. Within one printing job nine plates were fabricated vertically on the printing platform with a gap between each other of 3 mm. The samples are orientated perpendicular to the recoating direction, see Fig. 1.

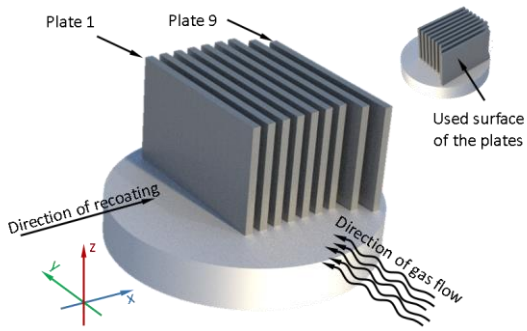

Fig. 1. Sample orientation at the printing platform during the L-PBF process

After the manufacturing, the samples were severed from the printing platform. In this investigation, two different pre-treatments of the 3D printed surfaces before laser cleaning are executed in order to analyse the influence of different amounts of residual powder on the laser cleaning performance. First the major amount of the loose powder is removed by suctioning the surfaces. Half of the samples were put additionally into an ultrasonic bath for 5 minutes, which was equipped with ethanol in order to extract the still residual lose powder particles.

Laser cleaning was carried out with a short pulse fibre laser in the nanosecond range of the type TRUMPF TruMark 5020 with an average power of 20 W. It is implemented in the 4-axis laser cell TruMark Station 5000, see Fig. 3 a). The beam is guided two dimensionally by means of a scanner optics in combination with an f-theta lens with a focal length of 254 mm and a scan field of view of 180 X 180 mm². The optics is equipped with a motorized collimation unit to shift the focal position in the range of ± 24 mm. The resulting beam caustic was measured by means of a FM100 (Metrolux, Göttingen, Germany). The measured laser beam exhibits a beam quality M^2 of 1.6, a focal diameter of 102.4 µm and a beam divergence of 21.52 mrad. The existing beam diameter d_s and intensity profiles at the work piece surface depending on the focal position z in the range between + 2 mm and + 5 mm above the sample surface, used in this investigation, are shown in Fig. 2.

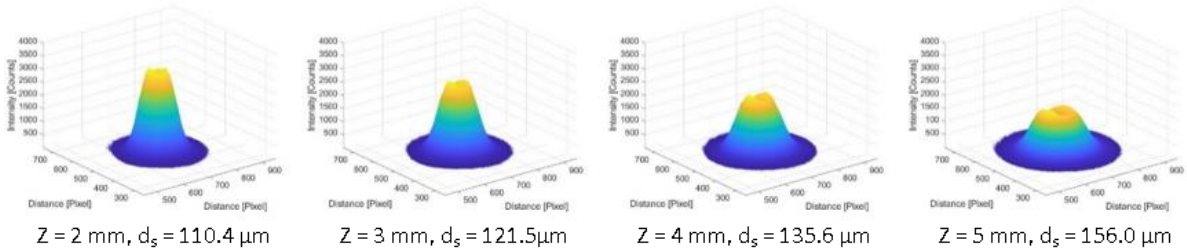

Fig. 2. Measured beam intensity profiles at the work piece surface depending on the focal position z in the range between + 2 mm and + 5 mm above the sample surface

The investigations on laser cleaning were performed at the re-coater averted side surface of the samples. For this purpose, the samples were clamped horizontally on the processing table of the machine. On each sample, eight laser cleaning test fields were created. The hatching direction is perpendicular orientated to the fabrication direction FD, Fig. 3 b).

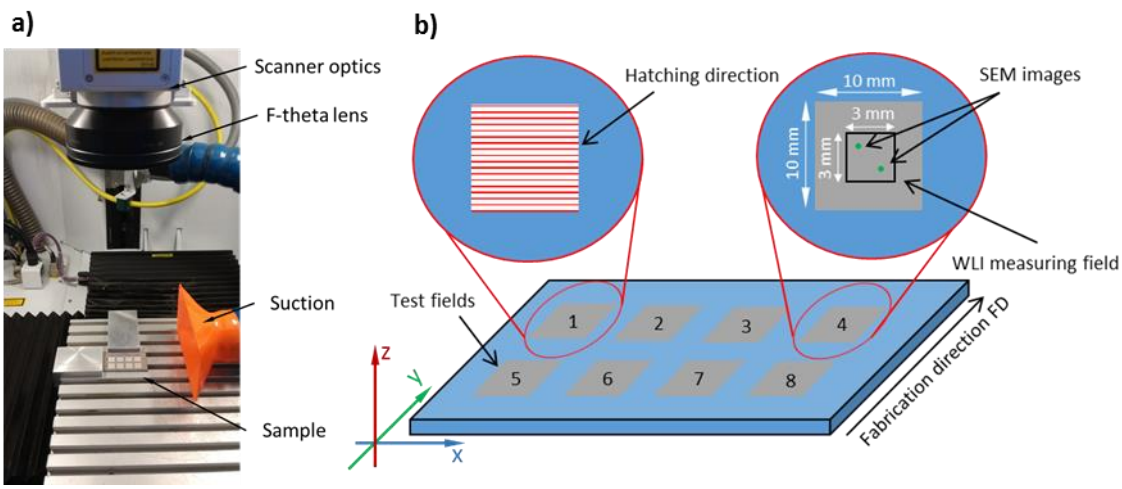

Fig. 3. a) experimental setup with mounted sample in TruMarkStation 5000, b) Test field positions and hatching direction on the LPBF printed samples, definition of WLI and SEM measuring positions

The surface behaviour is analysed at the initial state after 3D printing and after laser polishing optically by means of a microscope Axio Zoom V16 (Zeiss, Oberkochen, Germany) with a 50-fold magnification and a scanning electron microscope (SEM) of type LEO Gemini 1525 (Zeiss, Oberkochen, Germany) with a 500-fold, resp. 1000-fold magnification. The surface topography is analysed by use of a white light interferometer (WLI) NewView 8300 (AMETEK, Meerbusch, Germany) with a magnification of 20x.

In order to clearly define the test fields and ensure the identical measuring positions at the initial state and cleaned state, laser engraving is used to mark in the positions. WLI images with the dimension of 3*3 mm² are taken at the centre of the test fields. In diagonal direction at two positions (Fig. 3 b), marked with green dots, SEM images are taken.

The investigation on laser cleaning is carried out with a constant laser specific maximum average laser power P_{avg} of 20 W in combination with a scanning velocity v_s of 3000 mm/s and a hatch distance d_{hatch} of 34 µm. The parameter study is executed with a threefold cleaning pass. By varying the pulse repetition rate f_{rep} from 45 kHz up to 105 kHz, the pulse duration varies between 40 ns - 100 ns. The pulse energy E_p is in the range from 0.197 mJ – 0.456 mJ. Further, the single pulse Fluency F as well as the pulse and track overlap are adjusted by changing the focal position, respectively the beam diameter d_s, see Table 1.

Table 1 Varied laser parameters and resulting process parameters

Test Field Number	Beam Diameter d_s [µm]	Repetition Rate f_{rep} [kHz]	Pulse Duration t_p [ns]	Pulse Energy E_p [mJ]	Single Pulse Fluency F [mJ/mm²]	Pulse Overlap PO [%]	Track Overlap TO [%]
1	110.4	45	100	0.456	46.4	39.6	69.2
2	110.4	65	70	0.317	32.1	58.2	69.2
3	110.4	85	50	0.243	24.6	68.0	69.2
4	110.4	105	40	0.197	19.9	74.1	69.2
5	121.5	45	100	0.456	38.3	45.1	72.0
6	121.5	65	70	0.317	26.5	62.0	72.0
7	121.5	85	50	0.243	20.3	71.0	72.0
8	121.5	105	40	0.197	16.4	76.5	72.0
9	135.6	45	100	0.456	30.8	50.8	74.9
10	135.6	65	70	0.317	21.3	66.0	74.9
11	135.6	85	50	0.243	16.3	74.0	74.9
12	135.6	105	40	0.197	13.2	78.9	74.9
13	156	45	100	0.456	23.3	57.3	78.2
14	156	65	70	0.317	16.1	70.4	78.2
15	156	85	50	0.243	12.3	77.4	78.2
16	156	105	40	0.197	10.0	81.7	78.2

The resulting area rate as a function of the scanning velocity, hatch distance and number of cleaning passes amounts 20.4 cm²/min.

3. Results and discussion

3.1 Surface appearance and removal of dust and oxide layers

Cleaning the 3D printed surface in an ultrasonic bath results in a sporadic removal of particles from the surface structure. The entire surface becomes brighter due to the removal of smudge residues, see Fig. 4 b). Subsequent laser cleaning with a single pulse energy E_P 0.46 mJ of and a fluency F of 46.4 mJ/mm² produces a visible strong change in the surface topography due to remelting and structuring. The gloss level of the surface is strongly increased by removal of impurities and oxide layers (Fig. 4 c). The reduction of the single

pulse energy E_P to 0.20 mJ is accompanied by reduced structuring and surface remelting. An increasing laser beam diameter d_s to 156 µm causes only a minor change of the surface topography, but also an incomplete ablation of the brown coloured debris. A fluency F of 10 mJ/mm² leads to an insufficient removal of the residual particles and dust, respectively oxide layers (Fig. 4 f)).

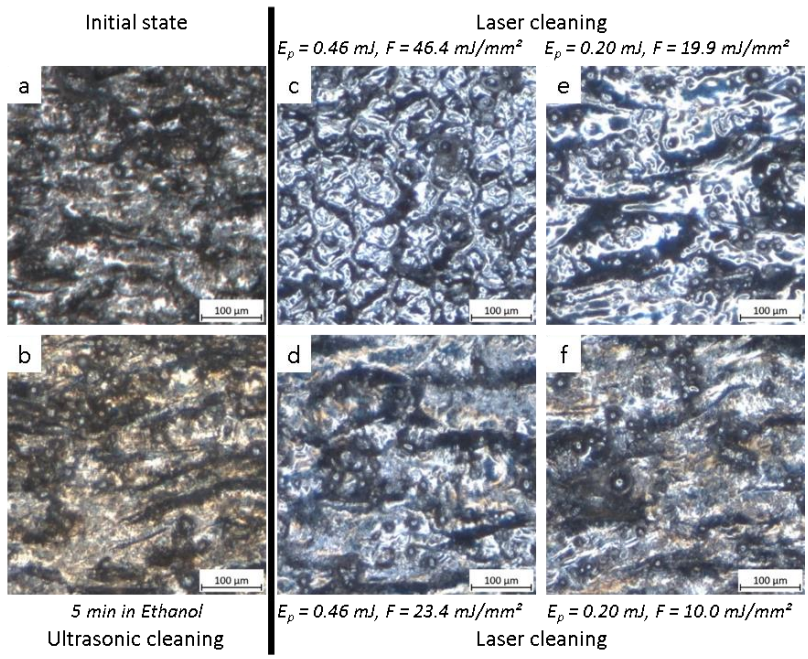

Fig. 4. Microscopic images, a) initial state after laser printing, b) with ultrasonic cleaning, c – f) laser cleaning with various pulse energy E_p and single pulse fluency F

3.2 Powder particle removal

The removal and ablation of powder particles, which are sintered or melted onto the component surface is analysed using SEM images of the initial state with ultra-sonic cleaning and after laser cleaning. Fig. 5 shows the initial state of the 3D printed surface with purple coloured powder particles, which could be removed depending on the used repetition rate f_{rep} and laser beam diameter d_s.

Laser cleaning achieves a partly ablation of the adherent powder particles. The ablation rate is strongly varying between the investigated fields within the parameter study. Repetition rates f_{rep} between 45 kHz and 85 kHz at a laser beam diameter of 110.4 µm, with high laser beam intensities I and fluency F achieves no particle removal. Less single pulse fluency F with pulse energies below than 0.317 mJ at a beam diameter of 156.0 µm also exhibits no ablated particles at the analysed section of the test field, due to insufficient energy input.

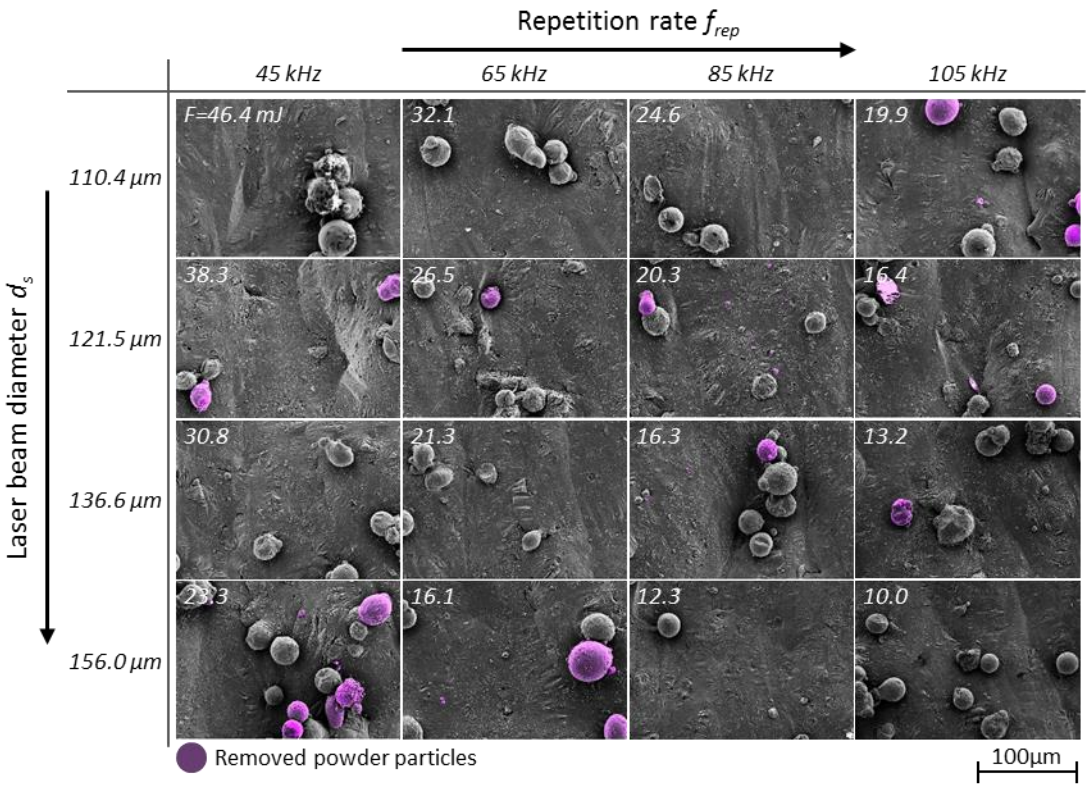

Fig. 5. SEM images of the initial surface after ultra-sonic cleaning with marked removed powder particles by laser cleaning

3.3 Process threshold fluencies

Due to varying single pulse fluency F between 46.4 mJ/mm² and 10.0 mJ/mm², by changing pulse energy E_p and laser beam diameter d_s, three different process regimes are existing, see Fig. 6. Laser cleaning with low fluencies F between 10.0 – 13.2 mJ/mm² causes a remelting of a thin surface layer on the adherent powder particles, while the surface of the component is still not melted. Fluencies F in the range of 16.1 – 23.3 mJ/mm² are resulting in a complete areal surface remelting, which can lead to an enhanced connecting area between the powder particle and the component surface as well as a fusion between the particles at itself, see Fig. 7 a) initial state, b) after laser cleaning. Fluencies F above 23.3 mJ/mm² causes an entire surface melting and structuring, red marked area at Fig. 6.

A more detailed view of the introduced surface structuring is given by the 3D topography WLI images of Fig. 8 a. At the maximum investigated fluency F of 46.4 mJ/mm² with a pulse overlap PO of 39.6%, a complete areal structuring of the surface topography with circular depressions with an extension of approx. 50 µm occurs. The resulting remelting zone at the powder particles and the sample surface are given by the microscopic images of the cross section with a 500-fold magnification at Fig. 7 c), d). The remolten surface layer exhibits an average melting depth of 3.3 µm and varies between 1.2 µm and 8.7 µm.

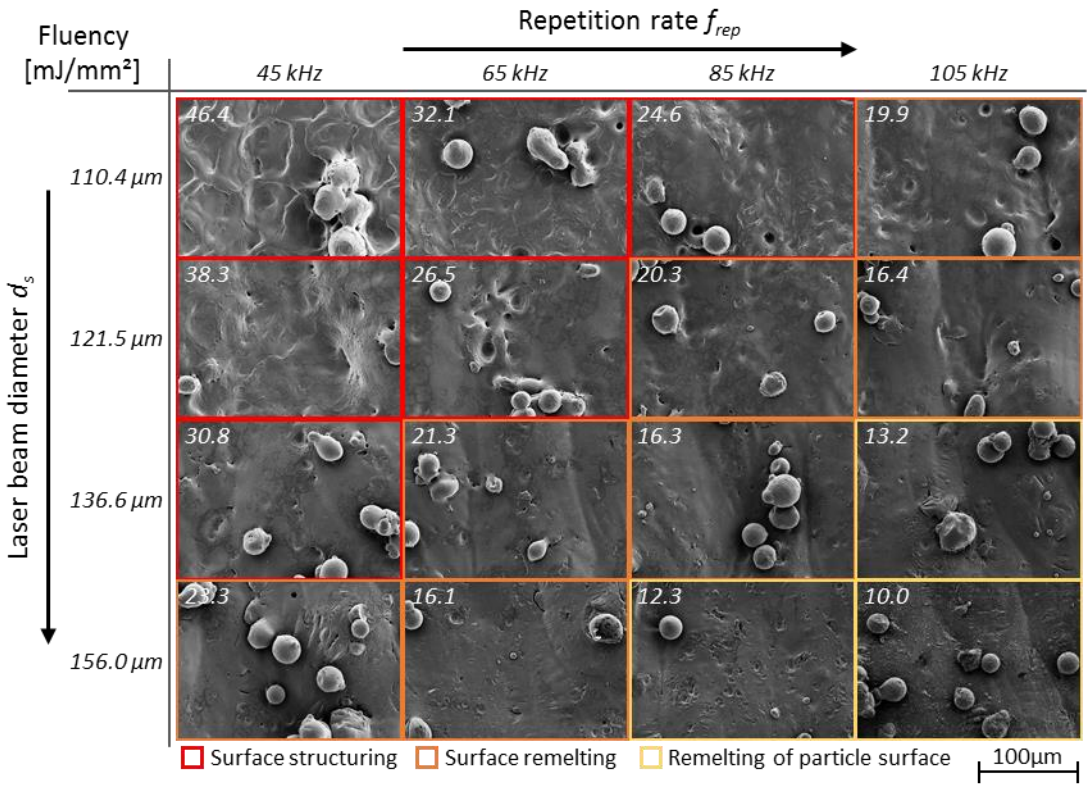

Fig. 6 SEM Images with a 500x magnification of the L-PBF surface after laser cleaning with surface structuring (red), surface remelting (orange), remelting of powder particle surface layer (yellow) depending on the single pulse fluency F

Within the increasing pulse repetition rate f_{rep} and decreasing pulse energy E_p the resulting surface treatment is changing from surface structuring to surface melting, between F = 24.6 - 19.9 mJ/mm².

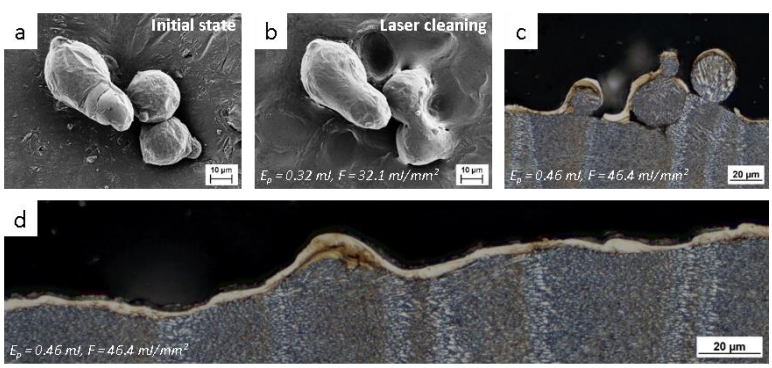

Fig. 7. a) & b) Fusion of powder particles and increased bonding surface due to particle melting, c) cross section through powder particles with a re-molten surface layer due to laser cleaning, d) cross section of re-molten surface layer with F = 46.4 mJ/mm²

With decreasing fluency due to the enhancement of the laser beam diameter the threshold fluency for surface structuring of F = 30.8 mJ/mm² is reached in combination with a beam diameter d_s = 135.6 µm. It results in small circular depressions with a diameter of 20-30 µm, respectively less than ¼ of the laser beam diameter, due to the highest beam intensity at the laser beam centre, see Fig. 8 b. The detailed differences between the initial surface and laser cleaned surface are given at the middle of Fig. 8.

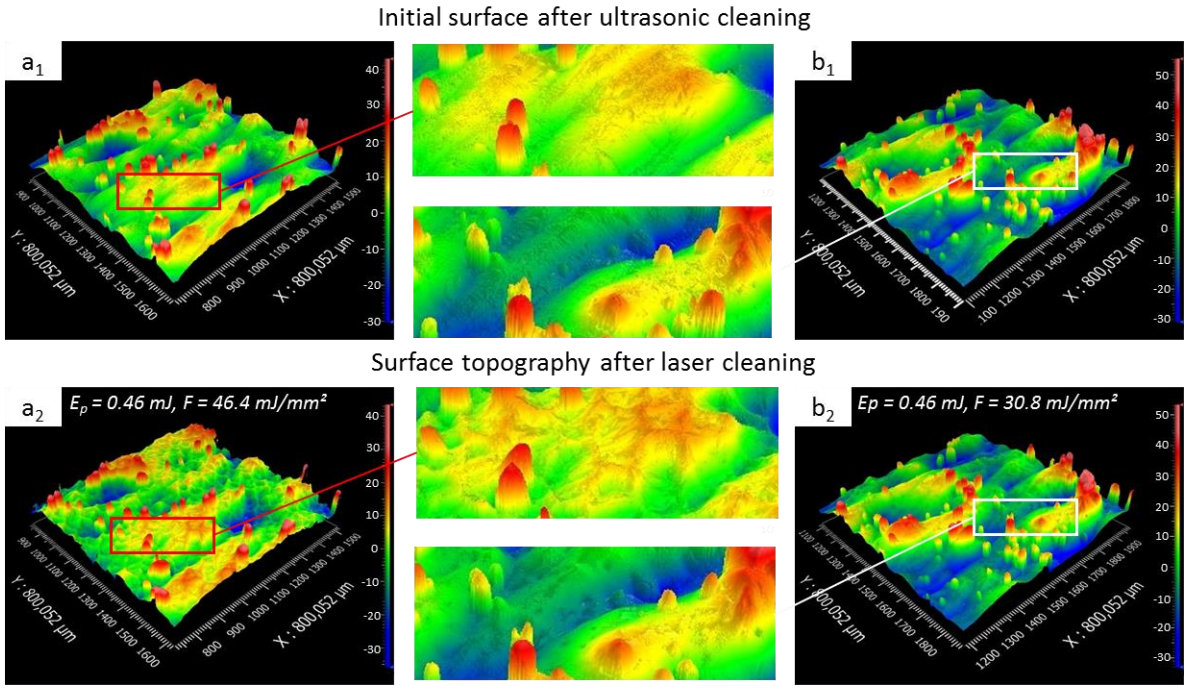

Fig. 8. 3D Topography of the initial surface after ultrasonic cleaning and resulting surface structures after laser cleaning with a hatch distance d_{hatch} of 34 µm, depending on the E_p and single pulse fluency F

A reduction of the fluency F < 30.8 mJ/mm², analysed by WLI, results in no further surface structuring, due to process temperatures below evaporation temperature of the base material.

4. Conclusion

Laser cleaning of L-PBF AlSi10Mg component surfaces can remove dust and oxide surface layers with area rates of 20.4 cm²/min. It achieves a partial and strongly varying ablation of adherent powder particles with single pulse fluencies F between 13.2 – 30.8 mJ/mm². A process threshold for melting a thin surface layer is determined above F = 13.2 mJ/mm². Fluencies F above 30.8 mJ/mm² causes a surface melting and structuring with a melting depth up to 8.7 µm and partly enhanced connecting area of the particles to the components surface. However, it is also visible, that some particles remain on the surface and, due to the surface remelting, generate a stronger bond between the particle and the surface. The ablation of those widely fused particles cannot be reached without changing the surface topography due to laser remelting or structuring.

Acknowledgements

H. Riegel acknowledges support by the German Federal Ministry of Education and Research, program 'FH-Impuls' (AddFunK, grant no. 03FH4I04IA) and 'FH-Invest' (Project FlexLight 4.0, Grant no. 13FH114N6).

References

Denti, Lucia; Sola, Antonella, 2019. On the Effectiveness of Different Surface Finishing Techniques on A357.0 Parts Produced by Laser-Based Powder Bed Fusion: Surface Roughness and Fatigue Strength, Metals, 12, 1284.

Guo, Lucy; Xie, Zhiqiang; Yao, Hong; Wang, Ying, 2017. A COMPARATIVE STUDY OF SURFACE CLEANING TREATMENTS FOR 3D PRINTED MEDICAL IMPLANTS, 2017, ASME Conference on Smart Materials, Adaptive Structures and Intelligent Systems, American Society of Mechanical Engineers et al. 2017 – Proceedings of the ASME Conference.

Kelly, Cambre N.; Evans, Nathan T.; Irvin, Cameron W.; Chapman, Savita C.; Gall, Ken; Safranski, David L., 2019. The effect of surface topography and porosity on the tensile fatigue of 3D printed Ti-6Al-4V fabricated by selective laser melting, Materials science & engineering. C, Materials for biological applications, 98, 726–736.

Kolb, T.; Mahr, A.; Huber, F.; Tremel, J.; Schmidt, M., 2019. Qualification of channels produced by laser powder bed fusion: Analysis of cleaning methods, flow rate and melt pool monitoring data. Additive Manufacturing, 25, 430–436.

Marimuthu, Sundar; Sezer, Hüsein Kürşad; Kamara, Alhaji M., 2018. Chapter 7 - Applications of Laser Cleaning Process in High Value Manufacturing Industries, Kohli, Mittal (Hg.) 2018 – Developments in Surface Contamination, 251–288.

Metelkova, Jitka; Ordnung, Daniel; Kinds, Yannis; van Hooreweder, Brecht, 2021. Novel strategy for quality improvement of up-facing inclined surfaces of LPBF parts by combining laser-induced shock waves and in situ laser remelting, 290.

Nasab, Milad Hamidi; Gastaldi, Dario; Lecis, Nora Francesca; Vedani, Maurizio, 2018. On morphological surface features of the parts printed by selective laser melting (SLM), Additive Manufacturing, 24, 373-377.

Pehlivan, Eren, Džugan, Jan, Fojt, Jaroslav, Sedlá˘cek, Radek, Rzepa, Sylwia, Daniel, Matej, 2020. Post-Processing Treatment Impact on Mechanical Properties of SLM Deposited Ti-6Al-4 V Porous Structure for Biomedical Application. Materials (Basel, Switzerland), 22, 5167.

Razab, Mohammad Khairul Azhar Abdul; Mohamed Noor, An'amt; Suhaimi Jaafar, Mohamad; Abdullah, Nor Hakimin; Suhaimi, Fatanah Mohamad; Mohamed, Mazlan; Adam, Noraina; Auli Nik Yusuf, Nik Alnur, 2018. A review of incorporating Nd:YAG laser cleaning principal in automotive industry, Journal of Radiation Research and Applied Sciences, 4, 393-402.

Seiffert, Gary; Hopkins, Carl; Sutcliffe, Chris, 2015. Comparison of high-intensity sound and mechanical vibration for cleaning porous titanium cylinders fabricated using selective laser Melting, Journal of biomedical materials research. Part B, Applied biomaterials, 105, 117-123.

Stark, M., 2021. Laserreinigen in High Speed, Lasermagazin 2021, 4, 2020, p. 8-11.
Townsend, A.; Senin, N.; Blunt, L., Leach, R.K.; Taylor, J.S, 2016. Surface texture metrology for metal additive manufacturing: a review, Precision Engineering, 46, 34-47.

Wang, Xiao; Xu, Mingyang; Wang, Zhanwen; Shen, Lida; Qiu, Mingbo; Tian, Zongjun; Ahsan, Muhammad; Wang, Changjiang, 2019. Properties of Jet-Plated Ni Coating on Ti Alloy (Ti6Al4V) with Laser Cleaning Pretreatment. Metals, 2, 248.

Zhu, Guodong; Wang, Shouren; Cheng, Wei; Wang, Gaoqi; Liu, Wentao; Ren, Yuan, 2019. Investigation on the Surface Properties of 5A12 Aluminum Alloy after Nd: YAG Laser Cleaning, Coatings, 9, 578.